

53-93

104979

P. 16

N92-29367

# A Nanoradian Differential VLBI Tracking Demonstration

R. N. Treuhaft and S. T. Lowe  
Tracking Systems and Applications Section

*The shift due to Jovian gravitational deflection in the apparent angular position of the radio source P 0201+113 was measured with very long baseline interferometry (VLBI) to demonstrate a differential angular tracking technique with nanoradian accuracy. The raypath of the radio source P 0201+113 passed within 1 mrad of Jupiter (approximately 10 Jovian radii) on March 21, 1988. Its angular position was measured 10 times over 4 hours on that date, with a similar measurement set on April 2, 1988, to track the differential angular gravitational deflection of the raypath. According to general relativity, the expected gravitational bend of the raypath averaged over the duration of the March experiment was approximately 1.45 nrad projected onto the two California-Australia baselines over which it was measured. Measurement accuracies on the order of 0.78 nrad were obtained for each of the ten differential measurements. The  $\chi^2$  per degree of freedom of the data for the hypothesis of general relativity was 0.6, which suggests that the modeled dominant errors due to system noise and tropospheric fluctuations fully accounted for the scatter in the measured angular deflections. The  $\chi^2$  per degree of freedom for the hypothesis of no gravitational deflection by Jupiter was 4.1, which rejects the no-deflection hypothesis with greater than 99.999-percent confidence. The system noise contributed about 0.34 nrad per combined-baseline differential measurement and tropospheric fluctuations contributed about 0.70 nrad. Unmodeled errors were assessed, which could potentially increase the 0.78-nrad error by about 8 percent. The above  $\chi^2$  values, which result from the full accounting of errors, suggest that the nanoradian gravitational deflection signature was successfully tracked.*

## I. Introduction

This article describes the first demonstration of a multi-source, wide-field very long baseline interferometry (VLBI) tracking technique, with temporally differential accuracies on the order of 1 nrad. In the standard mode of spacecraft angular tracking, called Delta Differential One-Way Ranging ( $\Delta$ DOR), the VLBI delays from a target space-

craft and one reference radio source are differenced in order to cancel common mode errors. An extension of this technique to include observations of multiple reference sources along with that of the target was proposed to improve on  $\Delta$ DOR performance [1]. As compared with typical  $\Delta$ DOR errors of 10-30 nrad, the multiple source, or "local reference frame," approach yields 1-nrad performance; the demonstration reported here was the first test of the mul-

tiple source approach. The sensitivity of the DSN, coupled with wide recorded and spanned bandwidths for the VLBI data, enables a single angular determination with the multisource observation strategy in approximately the same amount of time (approximately 30 minutes) required for a single  $\Delta$ DOR measurement with the narrow-bandwidth operational system.

In this demonstration, a natural source rather than a spacecraft was used as the target. In the first phase of demonstrating advanced angular tracking techniques, natural radio sources have frequently been used as targets instead of spacecraft [2,3]. The principal reasons for using natural sources are that (1) they exist in sufficient number and strength that a variety of target-reference source geometries are available at any time and (2) their "trajectories" are well known. In most natural source demonstrations, the goal is to see how closely a stationary target can be tracked. In this demonstration, the goal was to track the angular shift of the target source, resulting from planetary gravitational deflection, between two epochs. The angular position of the radio source P 0201+113 was measured ten times during each of two VLBI sessions, on March 21, 1988, and April 2, 1988. According to general relativity, the proximity of the target's raypath to Jupiter (1 mrad, or 10 Jovian radii), on March 21, 1988, produced an average gravitational deflection of about 1.45 nrad. On April 2, 1988, the raypath passed within about 3 degrees of Jupiter, which produced an expected deflection of less than 0.10 nrad, and the same observation schedule was repeated to attempt to track the differential gravitational signature. This differential signature was equivalent, for example, to a spacecraft motion of about 1 km at Jupiter between the March and April sessions. It has been shown, for example [4], that tracking at this level on approach to Jupiter would improve the determination of time of arrival and altitude above Io for Galileo.

During the period of mutual visibility (about 4 hours), the near-occultation event was observed ten times over two California-Australia (approximately 10,600-km) DSN baselines, with DSS 13, DSS 15, and DSS 43. Along with the target source, P 0201+113, several other sources were observed to estimate parameters characterizing clock, Earth rotation, and tropospheric effects [1]. Because the session-to-session *differences* in the angular positions of P 0201+113 were inferred from the VLBI data, the results were largely insensitive to stationary radio source position or structure uncertainties. The results were also largely insensitive to any other error source, such as antenna deformation, which is a function of antenna position, and therefore repeats with the same sidereal schedule. Details of the experimental procedure are presented in Section II

following a description of high-precision astrometric VLBI tracking below.

In astrometric VLBI tracking measurements, the angular position shift of a radio source from its expected or a priori value is inferred from the residual geometric delay.<sup>1</sup> The geometric delay is the difference between the arrival times, at each station of a baseline, of an electromagnetic wavefront from a radio source, which can be either a spacecraft or natural radio source. In this article, the geometric delay is defined to be positive if the wavefront arrives at Station 2 later than Station 1. The residual geometric delay for a single observation,  $\Delta\tau_g$ , is defined here to mean the delay due only to a shift  $\Delta s_p$  of the apparent source coordinate from its expected value, projected onto the baseline. The quantities  $\Delta s_p$  and  $\Delta\tau_g$  are related by (see, for example, [1]):

$$\Delta s_p = -\frac{c\Delta\tau_g}{B_p} \quad (1)$$

where  $B_p$  is the projection of the baseline onto the plane of the sky and  $c$  is the speed of light. The baseline vector, of which  $B_p$  is a component, points from Station 1 to Station 2. In the absence of measurement or modeling errors,  $\Delta s_p$  includes contributions from gravitational deflections induced by masses close to the raypath, and from radio source position and structure uncertainties. For spacecraft measurements,  $\Delta s_p$  also contains position departures from those given by a priori trajectories. In this analysis, solar deflection has been modeled in the a priori estimates of the geometric delay. The gravitational deflection signatures contributing to  $\Delta\tau_g$ , and therefore to  $\Delta s_p$ , are due only to Jupiter. The accuracy of the solar deflection modeling will be discussed in Subsection V.B. Special relativistic effects have also been modeled. In the differences between  $\Delta s_p$  determined from two sessions at the same sidereal time, stationary position and structure errors largely cancel, while the changes in gravitational signatures between the two sessions remain. In this natural source demonstration, the differences in gravitational signatures between the March and April sessions mimic unmodeled differential spacecraft motion. The set of measured differences in  $\Delta s_p$  are the final result of this demonstration. It will be shown below that these differences,  $\delta\Delta s_p$ , arise primarily from (1) the difference in the strength of Jovian gravitational deflection between the two sessions and (2) modeled stochastic errors.

<sup>1</sup> The term *residual* used throughout this article means the difference between the measured value of a quantity and an a priori estimate.

According to general relativity, the contribution to the terrestrially measured  $\Delta\tau_g$  due to the curvature of space-time around a spherically symmetric body of mass  $M$  is approximately

$$\Delta\tau_{g,rel} = \frac{2MG}{c^3} \ln \frac{r_1 + \vec{r}_1 \cdot \hat{k}}{r_2 + \vec{r}_2 \cdot \hat{k}} \quad (2)$$

where  $G$  is the gravitational constant equal to  $6.67 \times 10^{-8} \text{ cm}^3/\text{gm}\cdot\text{s}^2$ ,  $\vec{r}_i$  is the vector pointing from the center of the gravitating body to the  $i$ th station of the baseline, and  $\hat{k}$  is the unit vector pointing from the center of the gravitating body to the radio source. A term which differentially cancels between two observations at equal sidereal times has been dropped. This term, which compensates for the coordinate time of flight increment due to the body's field at the Earth (e.g., [5,6]), is less than one picosecond for Jupiter, even without differential cancellation.

In the next section, the experimental approach and details will be given. Sections III and IV describe the analysis procedures and the results, respectively. Section V enumerates unmodeled error sources, and Section VI contains conclusions and future directions.

## II. Experimental Approach

### A. The Local Reference Frame VLBI Technique

In the local reference frame technique, the residual geometric delay of a target radio source is inferred from VLBI observations of the target and several reference sources. For the target observation, the *measured* residual delay between the two antennas,  $\Delta\tau$ , contains the desired geometric contribution,  $\Delta\tau_g$ , along with other unwanted delay effects caused by errors in clock, Earth rotation, and troposphere characterizations. The basic idea of the VLBI technique used here is, for each of the target observations in a single experiment, to first separate the  $\Delta\tau_g$  component of  $\Delta\tau$  from other contributions to the measured target interferometric delay. From the set of  $\Delta\tau_g$ 's, a set of apparent angular deflections,  $\Delta s_p$ 's, are inferred, as indicated by Eq. (1). This procedure is then repeated for a later experiment and the  $\Delta s_p$  determinations at equal sidereal times are differenced to form the final result, a set of differential apparent positions,  $\delta\Delta s_p$ 's. In order to understand the extraction of the target residual geometric delay from the measured residual delay, the latter is expressed in terms of the residual geometric delay and other residual delays due to the effects mentioned above:

$$\begin{aligned} \Delta\tau = & \Delta\tau_g + \Delta\tau_{epoch} \\ & + \Delta\tau_{rate} + \Delta\tau_{rot1} + \Delta\tau_{rot2} \\ & + \Delta\tau_{trop1} + \Delta\tau_{trop2} + \epsilon \end{aligned} \quad (3)$$

In Eq. (3),  $\Delta\tau_{epoch}$  and  $\Delta\tau_{rate}$  are the delay errors associated with offsets in the clock epochs and rates between the two stations of the VLBI baseline. Delay errors due to uncalibrated Earth rotations about each of two axes orthogonal to the baseline are represented by  $\Delta\tau_{rot1}$  and  $\Delta\tau_{rot2}$ . The errors due to static tropospheric delays at each station are represented by  $\Delta\tau_{trop1}$  and  $\Delta\tau_{trop2}$  for Station 1 and Station 2, respectively. The quantity  $\epsilon$  represents all other errors not explicitly included. Associating one parameter with each explicit term in Eq. (3) means that a minimum of seven observations, one target and six reference scans are needed to estimate all indicated error parameters as well as the actual source shift. An expression similar to Eq. (3) can be written for each reference source scan, with  $\Delta\tau_g$  equal to zero. The geocentric delays are set to zero anticipating that stationary reference radio source position and structure uncertainties, which can each be as large as 5 nrad [7,8], will have identical contributions to reference residual geometric delays at corresponding epochs for each session. As with target observations, solar deflection effects have been modeled and removed from reference source delays (see Subsection V.B). By using Eq. (3) and the analogous equations for the reference source observations, the target  $\Delta\tau_g$  is extracted from the measured target and reference  $\Delta\tau$ 's. As noted above, repeating the observation sequence in a later session enables the extraction of  $\delta\Delta\tau_{g,rel}$ , the change in relativistic delay between observation sessions. This is actually accomplished by differencing  $\Delta s_p$  determinations extracted for the target during each session. An equation analogous to Eq. (3) can be written for the residual delay rates [1]. The temporally differential local reference frame technique can be regarded as an extension of the technique used to measure gravitational bending in [9] with one important distinction: Spatially differential observation errors are parameterized in terms of explicit physical effects (e.g., Earth rotation), as opposed to a parameterization linear in arc length separations on the sky.

### B. Experimental Details

As indicated by Eq. (3), multiple reference sources were used to estimate systematic delay effects for each of two experiments. The near-occultation event was observed from March 20, 1988, 23:30 UT, to March 21, 1988, 03:28 UT, and the entire observing schedule was repeated from

April 2, 1988, 22:39 UT to April 3, 1988, 02:37 UT. The Mark III VLBI data acquisition system [10] was operated at each station in mode A, which entails receiving and recording data from 28 2-MHz channels spread over the rf band. The centroids of the 2-MHz channels spanned two bands (S-band and X-band) for charged particle calibration. The spanned bands were approximately  $2285 \pm 19$  MHz and  $8450 \pm 53$  MHz. The characteristics of the three antennas used are summarized in Table 1.<sup>2,3</sup>

The target and reference radio sources observed are listed in Table 2. The table shows source coordinates and formal errors,<sup>4</sup> but the errors are preliminary and should be used to gauge relative measurement uncertainties of source coordinates. For a given source, these errors depend on its strength, the number of times it was observed, the baseline-source geometries, and the parameterization of the VLBI delays from which they were estimated in the global reference frame analysis. The true source position accuracy is probably never better than about approximately 2 nrad due to a number of possible systematic effects at that level. The baseline components used in the analysis are given in Table 3.

The observing sequence was divided into ten subsequences, one for each target measurement. In each subsequence, reference sources preceded and followed the target. The subsequences included target observations at the epochs given in Table 5 on results. The target observations at the first, fourth, and eighth epochs were surrounded by six other reference observations. The target observations for all other epochs were preceded and followed each by a single observation of the closest source, P 0202+14. As emphasized in Subsection V.D, in order to minimize error contributions due to radio source position or structure uncertainties, observation schedules were duplicated as much as possible between the March and April sessions. Therefore, if a reference scan was missed on an individual baseline for one epoch of a session, it was deleted from the analysis, for that baseline, at the corresponding epoch in the other session. All target scans were successful. One to

two reference source scans were deleted from each baseline. The determination of VLBI delays, rates, target positions, and modeled error parameters are described in the next section.

### III. Analysis Procedures

The standard procedures for analyzing VLBI data are discussed in [11,12,13]. In this section, the analysis of the gravitational deflection VLBI data will be discussed, with emphasis on the departures from the standard procedures. The extraction of interferometric delays and target source coordinates is followed by a discussion of the errors modeled in the analysis.

#### A. Extracting Interferometric Delays

From Eqs. (1), (2), and (3), it can be seen that the interferometric delays  $\Delta\tau$  are required to infer the measured  $\Delta\tau_{g,rel}$  and the resulting angular deflections  $\Delta s_p$  for each session. The first step in the VLBI processing was to obtain the interferometric group delays for each few-minute scan from the signals recorded at each station for each baseline. Since the integer cycle ambiguity associated with the group delay is much larger than that associated with the phase delay, group delays were used because they require less-accurate a priori information. The signals recorded at the stations included the broadband noise from the radio sources, background noise, and phase calibration tones to measure instrumental stability. Interferometric group delays were determined by cross correlation of the radio source data at the JPL/Caltech Block II processor [14]. Phase calibration signals were also extracted at the correlator. Both interferometric and phase calibration delays were refined with post-correlation fringe-fitting procedures.<sup>5</sup> A combination of phase calibration delays and short-baseline interferometric delays from the DSS 13-15 baseline were used to detect and correct significant instrumental effects in the long-baseline data. The corrected group delays were then used to estimate target source coordinates for the March and April sessions, as described below.

#### B. Extracting Source Coordinate Shifts by Parameter Estimation

The ultimate product of the data analysis is the set of projected, differenced source coordinate shifts of P 0201+113,  $\delta\Delta s_p$ , due to  $\delta\Delta\tau_{g,rel}$  at each of the ten observation epochs. The projected coordinate shift at each

<sup>2</sup> J. C. Breidenthal, *DSN/Flight Interface Design Handbook 810-5, Rev. D, vol. I, Module VLBI-10, Table 2* (internal document), Jet Propulsion Laboratory, Pasadena, California, June 1, 1990. See also S. D. Slobin, *Module TCI-10, Rev. E*; R. W. Sniffen, *Module TCI-20, Rev. C*; and S. D. Slobin, *TCI-30, Rev. D* in the same document.

<sup>3</sup> L. J. Skjerve, personal communication regarding the characteristics of DSS 13, Tracking Systems and Applications Section, Jet Propulsion Laboratory, Pasadena, California, February 1991.

<sup>4</sup> O. J. Sovers, personal communication regarding radio source catalog derived from JPL International Radio Interferometric Surveying and Crustal Dynamics Project data, Tracking Systems and Applications Section, Jet Propulsion Laboratory, Pasadena, California, February 1991.

<sup>5</sup> S. T. Lowe, *Theory of Post-Block II VLBI Observable Extraction* (internal document), Jet Propulsion Laboratory, Pasadena, California, March 1992.

epoch was determined by fitting the group delays and phase delay rates for all target and reference source observations to a set of projected source coordinate parameters for P 0201+113, as well as other parameters describing the errors in Eq. (3). The group delays were more important than the phase delay rates in the fit because, as discussed in the next section, typical delay errors were equivalent to about a 0.78-nrad error in the source coordinate shift per differential observation, while rate errors were equivalent to about a 30-nrad error.

Since VLBI delays are sensitive only to the component of the residual source position that lies along the baseline vector, this projection was estimated at each observation epoch for each session. The projection of the angular shift of P 0201+113 onto the baseline was determined by estimating the shifts of right ascension ( $\Delta\alpha$ ) and declination ( $\Delta\delta$ ) from a priori values. In order to constrain the source coordinate shifts to lie along the baseline projection,  $\Delta\alpha$  and  $\Delta\delta$  were forced to obey the following equation:

$$\Delta\alpha(t)(\hat{B}_z(t) - \hat{B}(t) \cdot \hat{s} \sin \delta) + \frac{\Delta\delta(t)}{\cos \delta}(\hat{B}(t) \times \hat{s})_z = 0 \quad (4)$$

where the residual right ascension and declination shifts are at epoch  $t$ , and  $\hat{s}$  is a unit vector in the direction of P 0201+113. The unit baseline vector  $\hat{B}$  and its  $z$ -component  $\hat{B}_z$  must be evaluated in the same celestial frame as  $\Delta\alpha$  and  $\Delta\delta$ . The constraint of Eq. (4) was used in the analysis because MODEST [13], the parameter estimation software used, was set up to estimate  $\Delta\alpha$  and  $\Delta\delta$ . An equivalent approach, which would have required writing new parameter estimation code, would have been to estimate the projected coordinate shifts,  $\Delta s_p(t)$ , directly, without using the intermediary shifts  $\Delta\alpha$  and  $\Delta\delta$ . Using the existing code, the values of  $\Delta s_p(t)$  were then calculated from  $\Delta\alpha$  and  $\Delta\delta$  according to

$$\Delta s_p(t) = \sqrt{\Delta\alpha^2(t) \cos^2 \delta + \Delta\delta^2(t)} \quad (5)$$

In addition to a projected residual source coordinate per epoch per session, at least one parameter per term in Eq. (3) was also estimated for each session. The equations for the partial derivatives of the delay and delay rate with respect to these parameters and source coordinate shifts are described in [13]. A more schematic treatment of the partial derivatives is given in the appendix of [1]. Four sets of station-differential clock epochs and rates were estimated for each session, over intervals of approximately

one hour. Earth rotation signatures were assumed to be linear over each session, during which a single set of three Earth rotation parameters was estimated. The rates of change of the Earth rotation parameters over the 4-hr sessions were inferred from 5-day differences in Earth rotation tables [15]. In MODEST, the rotation parameters were the magnitudes of the standard UT1, polar motion- $x$ , and polar motion- $y$  rotations. Since a single baseline is sensitive to only two components of Earth rotation, the three parameters were constrained as follows:

$$\hat{b}_x \Delta\theta_y + \hat{b}_y \Delta\theta_x - \hat{b}_z \Delta\theta_z = 0 \quad (6)$$

where  $\hat{b}_x$ ,  $\hat{b}_y$ , and  $\hat{b}_z$  are the components of the unit baseline vector in an Earth-fixed frame, and  $\Delta\theta_x$ ,  $\Delta\theta_y$ , and  $\Delta\theta_z$  are the  $x$ -pole,  $y$ -pole, and UT1 residual rotation magnitudes. The constraint of Eq. (6) ensures that the magnitude of the rotation about the baseline vector to which the data are insensitive is not estimated. The other estimated errors indicated by Eq. (3) are the static tropospheric delays at each station. A single zenith delay parameter per station per session was estimated from the data. The stochastic nature of the troposphere was included in the analysis with delay and rate troposphere covariance matrices described in the next subsection.

### C. Modeled Stochastic Errors

The errors assigned to the difference between projected source coordinate shifts for the March and April experiments were derived from the standard least-squares formalism (e.g., [16]). These errors in the final results are solely a function of the modeled covariance of the  $\epsilon$  error term in Eq. (3) and of the partial derivatives relating delay and rate observations to estimated parameters. Modeled stochastic observational errors, assumed to be independent between the two sessions, included only the white VLBI system noise and correlated tropospheric noise. The system noise error for each group delay and phase delay rate was calculated during the delay and rate extraction procedure [17],<sup>6</sup> and is based solely on the number of independent data samples in each scan and the observed correlated amplitude of the radio source over the baseline. Typical system noise errors were about 10–20 picoseconds per observation (0.34–0.68 nrad) for the delay and  $1.5 \times 10^{-15}$  to  $3 \times 10^{-15}$  sec/sec (0.58–1.16 nrad) for the delay rate. The system noise errors for intercontinental baselines using DSS 13 were about twice as large as those using DSS 15, which is consistent with the station characteristics of Table 1.

<sup>6</sup> Ibid.

The delay and rate covariance due to wet tropospheric fluctuations was calculated using the model of Treuhaft and Lanyi [18]. Their model accounts for spatial and temporal correlations of the tropospheric fluctuations. Standard wind speeds of 8 m/sec and wet tropospheric scale heights of 2 km were adopted. Because the model predicts that the tropospheric contribution to the delay rate data far outweighs the system noise contribution, the rate data were used to estimate the level of tropospheric fluctuations for each session. The key model parameter derived from the VLBI rates was the structure constant of the refractivity structure function. This structure function,  $D_\chi$ , for two points in the atmosphere separated by a distance  $r$ , is given by

$$D_\chi(r) = C^2 r^{2/3} \quad (7)$$

For each experiment, normalizing structure constants  $C$ , for each station, were chosen to make the reduced  $\chi^2$  of a rate-only fit equal to unity. Since the rate data were fit for each experiment separately, and since these data have a very small effect on the final astrometric result, as compared with the delays, this method of normalizing the troposphere covariance is essentially independent of the final differential angular result. It is therefore an a priori method of estimating the error due to tropospheric fluctuations and does not use the consistency of the final result to scale the assigned errors. If the rms rate scatters induced by the troposphere over each of the California stations are assumed to be equal, then the short (approximately 21-km) baseline can be used to infer the level of fluctuation in California. The long baseline rates can then be used to determine the Australia fluctuation contribution. The values of the derived single-station rms delay rates  $\sigma_{dr}$  and structure constants  $C$  are given in Table 4 for the two locations.

These structure constants were used to calculate troposphere observation covariance matrices for each baseline, for each session. These matrices were added to the diagonal system noise matrices to form the total observation covariance in the estimation of the  $\Delta s_p$ 's. In combining the baselines from a single session, the delay and delay-rate system noise errors from each baseline can be considered independent, but the tropospheric noise is correlated between baselines. The correlation arises because the two baselines share the common Australia station, and to a lesser degree, because the California stations are separated by 21 kilometers. The tropospheric correlations between observations on different baselines were explicitly included in the analysis. Assuming that tropospheric fluctuations in California and Australia are uncorrelated, the tropo-

sphere covariance matrix element between the  $i$ th VLBI delay of the DSS 13-43 baseline  $\tau_{13-43}$ , and the  $j$ th delay of the DSS 15-43 baseline  $\tau_{15-43}$ , is given by

$$\text{cov}(\tau_{13-43,i}, \tau_{15-43,j}) = \text{cov}(\tau_{43,i}, \tau_{43,j}) + \text{cov}(\tau_{13,i}, \tau_{15,j}) \quad (8)$$

where  $\text{cov}$  indicates the covariance between the two tropospheric delays in the argument, and  $\tau_{43,i}$ , for example, is the tropospheric delay at DSS 43 for the  $i$ th scan.

The level of error induced by the tropospheric fluctuations, assuming the structure constants in Table 4, was approximately 0.70 nrad for each differential measurement. This combines with an average system noise of about 0.34 nrad to give a total error of about 0.78 nrad per differential observation for the combined baseline system. Because the modeled troposphere covariance downweights delay rate measurements in accordance with the  $\sigma_{dr}$  values in Table 4, the delay rates are much less powerful in determining the final differential angles than the delays. Delay rates alone would have determined angular deflections with accuracies worse than 30 nrad per differential measurement.

## IV. Results

The results of the gravitational deflection measurements are shown in Figs. 1(a), 1(b), and 1(c). Figures 1(a) and 1(b) are plots of the measured angular differences,  $\delta\Delta s_p$ , between the March and April experiments on the baselines between DSS 13 and DSS 43, and between DSS 15 and DSS 43, respectively, as a function of Universal Time for the March experiment. Figure 1(c) shows the combined result for the two baselines, accounting for tropospheric correlations between baselines as described by Eq. (8). The curved lines of Fig. 1 show the prediction of general relativity for Jovian deflection, which can be obtained from Eqs. (1) and (2), and the horizontal, zero-deflection line is shown for reference. The general relativity curve decreases with time largely because the *projection* of the apparent coordinate shift on March 21 decreased as the baseline vector rotated. The unprojected effect decreased by approximately 10 percent over the 4-hour session, due to the decreasing colinearity of P 0201+113, Jupiter, and the Earth. The larger error bars at earlier epochs are due to low-elevation observations in Australia, where tropospheric fluctuations were strongest, as can be seen from Table 4. In order to produce Figs. 1(a) and 1(b), the parameters discussed after Eq. (5) were estimated along with the values of  $\Delta s_p$ . In order to produce

the combined-baseline solution of Fig. 1(c), the identical set of parameters was estimated, with an additional set of clock parameters to account for the independence of the clocks at DSS 13 and DSS 15.

Table 5 shows the results in numerical form. The values of the reduced  $\chi^2$ ,  $\chi_\nu^2$ , of the data about the general relativity and zero-deflection curves are given in Table 6 for each baseline and the combined result. In these  $\chi_\nu^2$  calculations, correlations are included between the values of  $\Delta s_p$  estimated at different epochs within each experiment. The  $\chi_\nu^2$  for the general relativity curves are all within one standard deviation of unity for the  $\chi_\nu^2$  distribution with 10 degrees of freedom. Based on the combined no-Jovian-deflection  $\chi_\nu^2$  of 4.1, that hypothesis is rejected with greater than 99.999-percent confidence, given the error modeling discussed in the previous section. The rms scatter of the combined result about the hypothesis of general relativity was 0.76 nrad. This is a measure of the demonstrated tracking accuracy per data point, or per 25- to 30-minute time interval. The  $\chi_\nu^2$  values for general relativity and no-Jovian deflection were subject to shifts of 0.2 and 0.4, respectively, when plausible modeling variations were tried. An example of one such variation was the alteration of the wind vector direction in the troposphere covariance calculation.

## V. Unmodeled Error Contributions

In the next few subsections, the levels of possible errors not included in the estimated or modeled error terms of Eq. (3) will be explored.

### A. Stochastic Behavior of Clocks and Earth Rotation

As described in Section III.B, both clock and Earth rotation effects were characterized with linear trends. In the case of the clocks, both the slope and intercept of the linear trend were estimated. Clock epochs and rates were estimated over approximately one-hour periods to remove the stochastic wandering of the hydrogen maser standards used at the DSN stations. This characterization is only an approximation of the actual stochastic clock behavior. Typical DSN clocks have Allan standard deviations between  $10^{-15}$  sec/sec and  $10^{-14}$  sec/sec [19], over time spans of a few thousand seconds. The clock rate parameters,  $\Delta\tau_{rate}$  of Eq. (3), estimated from the short-baseline analyses, implied an approximate single-station Allan standard deviation of  $5 \times 10^{-15}$  sec/sec. Simulations were performed to determine the effect of clock behavior characterized by Allan standard deviations with tempo-

ral dependences,<sup>7</sup> normalized to the short-baseline results. The simulations showed that deviations from the piecewise linear clock behavior contributes about 0.05 nrad of additional error to angular deflection estimates of Fig. 1(c). This angular error is much smaller than that expected from either system noise or the troposphere, which is why stochastic clock behavior was not modeled.

Earth rotation stochastic behavior was also modeled as linear due to similar reasoning. The variation of Earth rotation offsets during the 4-hour sessions was assumed to be equal to that derived from the published rate over 5-day periods surrounding each epoch [15]. Earth rotation rates over 4-hour periods can differ from those nominal 5-day rates by less than 5 nrad per 4-hour observing schedule. A sensitivity analysis showed that such a departure in Earth rotation rate would contribute less than 0.10 nrad of error to the estimated source coordinate shifts in Fig. 1(c).

### B. Solar Deflection Modeling

One possible contribution to the results of Fig. 1 is the incomplete removal of solar gravitational bending. If the solar gravitational deflections from each day, of both target and reference sources, were not removed, the apparent differential angular deflections of P 0201+113 between sessions would have been on the order of 50 nrad. Therefore, accurate solar gravitational deflection modeling is needed to separate the Jovian effect from that of the Sun. In addition to analytically confirming the general relativity calculation in the modeling segment of MODEST [13],<sup>8</sup> an empirical test of the solar deflection model was performed by considering another source in the schedule, P 0202+14, as the target. This source is 4 degrees away from P 0201+113 and from Jupiter and should therefore show no planetary gravitational deflection signature between the two sessions. This test, although consistent with zero deflection for P 0202+14, was a very weak one. The correlations between the deflection results for P 0202+14 and those for P 0201+113 were very high because both results came from essentially the same data. The P 0202+14 solution is mentioned to report that this obvious test was tried, and that it was consistent with accurate solar modeling. However, the analytic check of the MODEST modeling is a much stronger reason to doubt solar gravitational modeling errors. The analytic check showed that the solar modeling was accurate to better than about 3 picoseconds,

<sup>7</sup> J. B. Thomas and R. N. Treuhaft, personal communication regarding the treatment of relativity by MODEST software, Tracking Systems and Applications Section, Jet Propulsion Laboratory, Pasadena, California, October 1990.

<sup>8</sup> Ibid.

or about 0.10 nrad, for a single epoch, which should be regarded as an upper bound for the differential result. The calculated Jovian deflection in Fig. 1 is accurate to a much higher level.

The level of solar deflection for both target and reference sources mentioned above suggests that these data could have been analyzed to determine solar deflection to an accuracy on the order of one percent. As a consistency check, the data set was reanalyzed to solve for the  $\gamma$  parameter of relativistic gravitational theories [20]. Based on the differential solar deflection signatures between the March and April sessions, due to the motion of the Earth about the Sun between those sessions,  $\gamma$  was determined to be equal to  $1.011 \pm 0.036$ . This value is consistent with general relativity's prediction that  $\gamma$  be equal to unity, and the error is equivalent to a 1.8-percent measurement of solar deflection.

### C. Propagation Through Jupiter's Magnetosphere

Another possible mechanism contributing to the measured deflections of Fig. 1 is refractive bending through Jupiter's magnetosphere. Although this error source would not be a concern for demonstrations with sources far from Jupiter, it is described here because it is important in this experiment and could conceivably be of operational importance for a spacecraft in orbit about Jupiter. As noted in Section II.B, charged particle effects were calibrated by observing at S-band (2285 MHz) and X-band (8450 MHz). Magnetic fields or electron columnar contents (electron densities integrated along the direction of propagation) much larger than those found near Earth would require higher order corrections than the simple dual frequency method used here. From Voyager 1 measurements, the magnetic field at 10 Jovian radii, near the equatorial plane, is approximately 4 mG [21]. This field strength is about 100 times smaller than that of the field at the surface of the Earth. The differential field across the baseline is a few tenths of a milligauss. Voyagers 1 and 2 plasma wave measurements indicate that the equatorial electron content, differenced between the ends of a 10,000-km baseline, for a ray at 10 Jovian radii is about  $5 \times 10^{15}$  electrons/m<sup>2</sup> [22]. The presence of these baseline differential magnetic fields and electron columnar contents will cause delay errors equivalent to less than 0.001 nrad in the angular measurement, if the dual frequency approach to charged particle calibration is used.<sup>9</sup>

An empirical determination of the electron content along the line of sight through Jupiter's magnetosphere

can be obtained by using the VLBI data from the March and April sessions. In order to investigate the electron columnar content along the line of sight to P 0201+113, Fig. 2 shows the difference in electron columnar content between adjacent scans of P 0201+113 and P 0202+14 versus time, differenced between the March and April sessions. This double difference was formed to look for an increased charged particle columnar content along the line of sight to P 0201+113 during the March session. Differencing the electron content between sources compares the line of sight near Jupiter with one far (4 degrees) from Jupiter, and differencing between sessions reduces geometric effects due to the different slant angles through the ionosphere of the two raypaths. The electron contents of Fig. 2 are derived from the DSS-15 to DSS-43 S- and X-band delays. The electron content at time  $t$ ,  $TEC(t)$ , is calculated from the residual group delays at S-band and X-band,  $\Delta\tau_S(t)$  and  $\Delta\tau_X(t)$  as follows:

$$TEC(t) = \frac{mc}{2\pi e^2} \frac{\omega_S^2 \omega_X^2}{\omega_X^2 - \omega_S^2} (\Delta\tau_S(t) - \Delta\tau_X(t)) \quad (9)$$

where  $m$  is the electron mass in grams,  $c$  is the vacuum speed of light in centimeters per second,  $e$  is the electron charge in statcoulombs, and  $\omega_S$  and  $\omega_X$  are the S- and X-band centroid frequencies [23]. From the figure, it can be seen that the temporally differential columnar content differs between the two sources by less than  $10^{15}$  electrons/m<sup>2</sup>, or about an order of magnitude lower than the number derived from the literature above. Since the raypath of the target passed 10 Jovian radii to the north of the planet, the baseline differential electron content derived from the equatorial Voyager data should be regarded as an upper bound. In Fig. 2, there may be some ionospheric contribution to the observed electron contents due to the changes in Sun-radio source angles between the two sessions, and a possible change of ionospheric activity between the two sessions. Both of these effects would cause an imperfect cancellation of the geometric ionospheric effect mentioned above and would further lower the differential electron content ascribed to the Jovian magnetosphere. This empirical study of the magnetospheric electron content suggests that the 10-picoradian error derived from the Voyager data is probably an overestimate and not a concern for the error budget of this experiment.

### D. Radio Source Position and Structure Errors

There are two classes of radio source position and structure errors: stationary and fluctuating. As has been mentioned, stationary reference radio source position or structure errors identically cancel between sessions in which the

<sup>9</sup> S. T. Lowe, op. cit.

observation sequence is exactly repeated, as long as the equations that relate measured residual delay to parameter shifts are also identical for each session. This cancellation occurs because any delay or delay rate effect that exactly repeats will affect the apparent coordinates of P 0201+113 identically in both sessions. If the observation sequence is changed, or if the analysis equations are changed, even delay and delay-rate position or structure effects which side-really repeat between schedules will cause errors in the final results [1]. Stationary radio source structure errors can therefore affect the differential results presented here because: (1) Beginning and ending sidereal times for each scan differed slightly between the March and April epochs, and, as indicated in Table 4, (2) a different ratio of tropospheric error to system noise error was ascribed to each session. The effect of stationary reference source position errors on the measured angular deflection of P 0201+113 was calculated by assuming stationary position errors and determining their effect on the final result for each epoch. It was found that reference sources temporally close to the target observation in question were most important and that the incurred error in the target position was on the order of 10 percent of the average stationary errors in those reference sources. By conservatively considering possible systematic errors, an average accuracy of 2.42 nrad was ascribed to the radio source coordinates in Table 2. It follows that errors on the order of 0.24 nrad could result from typical stationary reference source uncertainties. While data editing could have reduced this error further by making the observation sequences more similar to each other, it did not seem warranted for an error of this size. It is also important to note that had the resulting sensitivity to stationary errors been higher, the inequality of the observable troposphere covariance between sessions could have been adjusted. In this set of experiments, using a suboptimal covariance matrix for the troposphere of one experiment to make it more equal to that of the other was deemed unnecessary. In other differential experiments, the error incurred by the inequality of the tropospheric covariance matrix between sessions may be large. In that case, suboptimal tropospheric matrices may be adopted in order to desensitize the differential result to stationary reference source uncertainties; a trade-off between these two error sources must be considered.

The second type of radio source uncertainty is due to fluctuations of apparent source position due to a changing radio source structure, which results in an effective proper motion. From [24], it can be seen that average radio source position shifts due to structure changes are on the order of 5 nanoradians per year. Assuming that the apparent change in position is linear with time, over 13 days, 0.15 nrad of position change per source would be ex-

pected. Covariance studies show that these errors would propagate into about 0.10-nrad errors in the P 0201+113 coordinates. Thus, the combined stationary and fluctuating radio source coordinate errors could add about 6 percent to the nominal 0.78-nrad formal errors in this experiment.

### E. Geophysical Effects

The geophysical model used to calculate the residual delays of Eq. (3) contains many components which could conceivably contribute to a differential error between the two observation epochs. Delays due to the tides, baseline length uncertainties, ocean loading, and tropospheric mapping functions could change between epochs and must be removed in order to avoid aliasing into the gravitational deflection signature. Each of these effects was estimated with a sensitivity analysis, and they evidenced typical signatures of less than 0.05 nrad apiece. An overall error of 0.10 nrad is assigned to geophysical effects.

### F. Summary of Unmodeled Errors

Table 7 summarizes the unmodeled error effects. Added in quadrature, the unmodeled effects could contribute up to 0.32 nrad. The total unmodeled error could therefore add 8 percent to the 0.78-nrad modeled error. However, there is no indication from the  $\chi^2_\nu$  values of Table 6 that unmodeled errors were important in the analysis of these data.

It is worth noting that the accuracy of the ephemeris of Jupiter is not a concern for the analysis of this experiment. Errors in the Jovian ephemeris would change the general relativity curve of Fig. 1, which is obtained with Eqs. (1) and (2). The current ephemeris accuracy of Jupiter is about 200 nrad [25], which causes uncertainties in the theoretical curve of Fig. 1 at the level of less than 0.005 nrad. Conversely, the position of Jupiter in the radio reference frame is very poorly determined by this experiment, relative to the current ephemeris accuracy.

## VI. Conclusions

The technique of differential VLBI, over two DSN California-Australia baselines, was used to track the angular deflection of the raypath of P 0201+113 when it passed within 200 arcseconds (approximately 10 Jovian radii) of Jupiter. Two experiments were performed: one at the time of near-occultation and one 13 days later, when the raypath was about 3 deg from Jupiter. The results of Fig. 1(c) yield a  $\chi^2_\nu$  about the hypothesis of Jovian deflection of 0.6,

and are therefore consistent with Jovian gravitational deflection of the raypath. The  $\chi^2_\nu$  about the hypothesis of zero Jovian deflection is 4.1, which rejects that hypothesis at greater than the 99.999-percent confidence level, and suggests that the deflection was successfully tracked at the nanoradian level. The tracking demonstration involved estimating clock, Earth rotation, and tropospheric parameters from observations of a local reference frame of radio sources surrounding P 0201+113. Because the reference sources were many degrees from the target to be tracked, the experiments reported in this article demonstrate a wide-field differential astrometric tracking technique with 0.78-nrad accuracy.

The dominant errors in the measurements were white system noise due to sky and instrument background and correlated tropospheric noise. The effect of the white system noise can be calculated from the number of samples, or bits, cross-correlated in the VLBI processing and the observed correlated amplitude. The effect of the correlated tropospheric errors was assessed with a statistical model of tropospheric fluctuations. This model was normalized separately for each experiment and station by using the phase delay rate data from both the short and long baselines formed by the three stations. The system noise and tropospheric errors contributed about 0.34 nrad and 0.70 nrad to the final 0.78-nrad uncertainty per differential measurement. The values of  $\chi^2_\nu$  derived from the hypothesis of general relativistic, Jovian deflection suggest that these two modeled error sources fully account for observed errors in the final results. However, unmodeled effects due to the stochastic behavior of clocks and Earth rotation, solar deflection mismodeling, charged particles in Jupiter's magnetosphere, radio source position and structure errors, and geophysical effects could add approximately 8 percent to the 0.78-nrad uncertainty.

There are several improvements in observation and calibration strategies which could result in higher measurement accuracies for future wide-field astrometric experiments (for a more complete discussion, see [1]). If the highly accurate phase delay could be used instead of the group delay, the system noise error would be reduced by about two orders of magnitude to about 10 prad. Efforts to resolve phase-delay ambiguities on intercontinental baselines are currently under way. The ultimate precision of this astrometric technique is determined by the system noise level of the phase delay measurement. It is therefore worth considering means for reducing other errors to that level. It is possible that water vapor radiometry [26,27] could be used to calibrate the wet tropospheric fluctuations, the other dominant error source. Refractivity fluctuations in the dry atmosphere will also contribute to the

astrometric error. The exact level of the dry fluctuation contribution has not been measured, but it is probably about a factor of 5-10 smaller than the wet fluctuation contributions. Barometric arrays or other radio metric techniques might be useful in calibrating the dry fluctuations. Finally, as noted in Section V, radio source structure fluctuations are important for differential measurements, made within a few weeks of each other, at the level of 0.10 nrad. For differential measurements made over longer time periods, the structure errors will exceed the 0.10-nrad effects reported in this article. If all other error sources have been reduced to the approximately 10-prad level, it may become necessary to account for radio source structure fluctuations, even over periods as short as a few days. In addition to mapping reference and target radio sources over time, another possibility, as yet unexplored, is to add structure parameters to Eq. (3) and estimate time-varying structure effects directly from the astrometric VLBI observations. This possibility will be explored in the Advanced System Program next fiscal year.

An interesting byproduct of this tracking technique is the measurement of solar gravitational deflection. Because the solar gravitational effect on the data presented here was on the order of 50 nrad (the target was about 25 degrees from the Sun), this experiment constituted a 2-percent solar gravitational measurement. If the target were a few degrees from the Sun, the solar deflection could be measured, with better than 0.1-percent accuracy, with two experiments of the duration of those reported here. Solar plasma fluctuations would be a possible obstacle, but with sufficient signal strength, it may be possible to freeze the solar plasma fluctuations on short time scales in conjunction with dual frequency calibration. If successful, repeated measurements near the Sun could begin to improve on the state-of-the-art measurement of the post-Newtonian  $\gamma$  parameter of gravity theories [28]. Proof-of-concept solar deflection experiments are currently supported by the TDA Science Office.

This demonstration was done with a natural radio source target, P 0201+113. A nanoradian-tracking demonstration on Galileo had been planned before the high-gain antenna availability became an issue. Unless high-gain transmission is restored, spacecraft system noise and charged particle errors incurred with the low-gain S-band downlink will make a 1-nrad Galileo demonstration virtually impossible. A key difference between the spacecraft and natural source targets is in the bandwidth of the received signals; spacecraft transmit tones, while natural sources are broadband in nature. Dispersive phase effects in the receiving electronics may therefore affect the target spacecraft and natural reference source signals differ-

ently. Studies of the dispersive nature of the DSN receiving electronics<sup>10</sup> will be necessary before demonstrating nanoradian accuracy on future spacecraft, such as Cassini.

Applications of nanoradian accuracy include Jovian ephemeris development on approach for Galileo, ring analysis at Saturn for Cassini, and aerocapture approach trajectory optimization for missions to Mars. Temporally differential results have been presented in this article. While temporally differential measurements frequently yield use-

ful navigation products (for example, Jovian ephemeris development on approach), absolute positions relative to solar system bodies are also needed. It should be noted that the radio source structure at the 5-nrad level and planetary position errors in the radio frame as high as 200 nrad limit some classes of body-relative measurements. Temporally differential high-accuracy results in the radio frame, however, are necessary precursors to nanoradian body-relative demonstrations. Temporally differential demonstration of the sort reported here address a large subset of the body-relative errors, namely system noise and atmospheric fluctuations; in fact, analysis of high-accuracy temporally differential measurements of planetary orbiters can locate those bodies in the radio frame.

<sup>10</sup> C. Edwards and K. Zukor, "Video Converter Local Oscillator Stability for Block I and Block II VLBI," JPL Interoffice Memorandum 335.1-90-055 (internal document), Jet Propulsion Laboratory, Pasadena, California, October 30, 1990.

## References

- [1] R. N. Treuhaft, "Deep Space Tracking in Local Reference Frames," *TDA Progress Report 42-94*, vol. April-June 1988, Jet Propulsion Laboratory, Pasadena, California, pp. 1-15, August 15, 1988.
- [2] B. K. Trinkle and S. M. Lichten, "Differential Very Long Baseline Interferometry for 50-nanoradian Deep Space Navigation," *Astrodynamicity 1985*, Proceedings of the Conference, Part 2 (A86-43201 20-12), edited by Kaufman et al., Univelt, Inc.: San Diego, California, pp. 1257-1276, 1986.
- [3] R. N. Treuhaft and B. K. Trinkle, "High Precision Navigation Demonstration With Extragalactic Radio Sources," *JPL Highlights*, Jet Propulsion Laboratory, Pasadena, California, pp. 62-63, 1986.
- [4] W. M. Folkner, "Navigational Utility of High-Precision Radio Interferometry for Galileo's Approach to Jupiter," *TDA Progress Report 42-102*, vol. April-June 1990, Jet Propulsion Laboratory, Pasadena, California, pp. 34-46, August 15, 1990.
- [5] M. H. Soffel, J. Muller, X. Wu, and C. Xu, "Consistent Relativistic VLBI Theory with Picosecond Accuracy," *Astronomical Journal*, vol. 101, pp. 2306-2310, June 1991.
- [6] B. Shahid-Saless, R. W. Hellings, and N. Ashby, "A Picosecond Accuracy Relativistic VLBI Model via Fermi Normal Coordinates," *Geophysical Research Letters*, vol. 18, pp. 1139-1142, June 1991.
- [7] O. J. Sovers, C. D. Edwards, C. S. Jacobs, G. E. Lanyi, K. M. Liewer, and R. N. Treuhaft, "Astrometric Results of the 1978-1985 Deep Space Network Radio Interferometry—The JPL 1987-1 Extragalactic Source Catalog," *Astronomical Journal*, vol. 95, pp. 1647-1658, June 1988.
- [8] P. Charlot, "Radio-Source Structure in Astrometric and Geodetic Very Long Baseline Interferometry," *Astronomical Journal*, vol. 99, pp. 1309-1326, April 1990.

- [9] E. B. Fomalont and R. A. Sramek, "A Confirmation of Einstein's General Theory of Relativity by Measuring the Bending of Microwave Radiation in the Gravitational Field of the Sun," *Astrophysical Journal*, vol. 199, pp. 749-755, August 1, 1975.
- [10] A. E. E. Rogers, R. J. Cappallo, H. F. Hinteregger, J. I. Levine, E. F. Nesman, J. C. Webber, A. R. Whitney, T. A. Clark, C. Ma, J. W. Ryan, B. E. Corey, C. C. Counselman, T. A. Herring, I. I. Shapiro, C. A. Knight, D. B. Shaffer, N. R. Vandenberg, R. Lacasse, R. Mauzy, B. Rayhrer, B. R. Schupler, and J. C. Pigg, "Very-Long Baseline Radio Interferometry—The Mark III System for Geodesy, Astrometry, and Aperture Synthesis," *Science*, vol. 219, pp. 51-54, January 7, 1983.
- [11] I. I. Shapiro, "Estimation of Astrometric and Geodetic Parameters," in *Methods of Experimental Physics, Part C*, edited by M. L. Meeks, Orlando, Florida: Academic Publishers, pp. 261-276, 1976.
- [12] T. A. Herring, "Precision and Accuracy of Intercontinental Distance Determinations Using Radio Interferometry," Ph.D. thesis, Hanscom Air Force Base, Massachusetts: Air Force Research Cambridge Laboratories, July 1983.
- [13] O. J. Sovers, *Observation Model and Parameter Partial for the JPL VLBI Parameter Estimation Software MODEST/1991*, JPL Publication 83-39, Rev. 4, Jet Propulsion Laboratory, Pasadena, California, August 1, 1991.
- [14] J. B. Thomas, *Interferometry Theory for the Block 2 Processor*, JPL Publication 87-29, Jet Propulsion Laboratory, Pasadena, California, October 15, 1987.
- [15] "IRIS Bulletin A (International Radio Interferometric Surveying)," *Earth Orientation Bulletin A*, vol. 53, 1988.
- [16] W. C. Hamilton, *Statistics in Physical Science*, New York: Ronald Press, p. 124, 1964.
- [17] A. R. Thompson, J. M. Moran, and G. W. Swenson, *Interferometry and Synthesis in Radio Astronomy*, New York: Wiley and Sons, 1986.
- [18] R. N. Treuhaft and G. E. Lanyi, "The Effect of the Dynamic Wet Troposphere on Radio Interferometric Measurements," *Radio Science*, vol. 22, March-April, pp. 251-265, 1987.
- [19] P. F. Kuhnle, "NASA/JPL Deep Space Network Frequency and Timing," *Proceedings of the Twenty-First Annual Precise Time and Time Interval Applications and Planning Meeting*, Redondo Beach, California, pp. 479-489, 1989.
- [20] C. M. Will and K. Nordtvedt, Jr., "Conservation Laws and Preferred Frames in Relativistic Gravity, Part I: Preferred-Frame Theories and an Extended PPN Formalism and Part II: Experimental Evidence To Rule Out Preferred-Frame Theories of Gravity," *Astrophysical Journal*, vol. 177, pp. 757-792, 1972.
- [21] N. F. Ness, M. H. Acuna, R. P. Lepping, L. F. Burlaga, K. W. Behannon, and F. M. Neubauer, "Magnetic Field Studies at Jupiter by Voyager 1—Preliminary Results," *Science*, vol. 204, pp. 982-987, June 1, 1979.
- [22] D. A. Gurnett, F. L. Scarf, W. S. Kurth, R. R. Shaw, and R. L. Poynter, "Determination of Jupiter's Electron Density Profile From Plasma Wave Observations," *Journal of Geophysical Research*, vol. 86, no. A10, pp. 8199-8212, 1981.
- [23] J. D. Jackson, *Classical Electrodynamics*, New York: Wiley and Sons, pp. 288-289, 1975.

- [24] R. W. Porcas, "Summary of Known Superluminal Sources," in *Superluminal Radio Sources*, edited by J. A. Zensus and T. J. Pearson, New York: Cambridge University Press, pp. 12-25, 1987.
- [25] A. E. Niell, X X Newhall, R. A. Preston, G. L. Berge, D. O. Muhleman, D. J. Rudy, J. K. Campbell, P. B. Esposito, and E. M. Standish, "Relating the Planetary Ephemerides and the Radio Reference Frame," *TDA Progress Report 42-81*, vol. January-March 1985, Jet Propulsion Laboratory, Pasadena, California, pp. 1-8, May 15, 1985.
- [26] G. M. Resch, D. E. Hogg, and P. J. Napier, "Radiometric Correction of Atmospheric Path Length Fluctuations in Interferometric Experiments in Radio Astronomy," *Radio Science*, vol. 19, January-February, pp. 411-422, 1984.
- [27] G. Elgered, J. L. Davis, T. A. Herring, and I. I. Shapiro, "Geodesy by Radio Interferometry—Water Vapor Radiometry for Estimation of the Wet Delay," *Journal of Geophysical Research*, vol. 96, pp. 6541-6555, April 10, 1990.
- [28] R. D. Reasenberg, I. I. Shapiro, P. E. MacNeil, R. B. Goldstein, J. C. Breidenthal, J. P. Brenkle, D. L. Cain, T. M. Kaufman, T. A. Komarek, and A. I. Zygielbaum, "Viking Relativity Experiment—Verification of Signal Retardation by Solar Gravity," *Astrophysical Journal, Part 2—Letters to the Editor*, vol. 234, pp. L219-L221, December 15, 1979.

**Table 1. Characteristics of the DSN antennas used in the gravitational deflection measurements.**

Antenna	Location	Diameter, m	System temperature, K	Efficiency, percent
DSS 13	Goldstone	26	30	45
DSS 15	Goldstone	34	20	72
DSS 43	Australia	70	20	66

**Table 2. Target and reference radio sources used in the gravitational deflection measurements.**

Source name	Right ascension			Declination			Right ascension error, msec	Declination error, mas
	hr	min	sec	deg	min	sec		
P 0201+113	02	03	46.65701	11	34	45.4107	0.03	0.6
P 0019+058	00	22	32.44122	06	08	04.2692	0.03	0.9
P 0106+01	01	08	38.77107	01	35	0.3179	<0.01	0.1
GC 0119+04	01	21	56.86167	04	22	24.7347	<0.01	0.2
CTD 20	02	37	52.40567	28	48	08.9904	<0.01	<0.1
GC 0235+16	02	38	38.93011	16	36	59.2750	0.01	0.1
OD 166	02	42	29.17090	11	01	00.7275	0.03	0.4
3C 454.3	22	53	57.74793	16	08	53.5610	<0.01	0.1

**Table 3. California–Australia DSN baseline vectors.**

Baseline	X, m	Y, m	Z, m	Length, m
DSS 13–43	-2109765.511	7337838.348	-7335705.773	10588085.819
DSS 15–43	-2107355.861	7324010.785	-7351418.891	10588930.183

**Table 4. Single-station delay rates and tropospheric refractivity structure function constants.**

Session	$\sigma_{dr}$ - California, psec/sec	$\sigma_{dr}$ - Australia, psec/sec	$C$ - California, $10^{-7} \text{ m}^{-1/3}$	$C$ - Australia, $10^{-7} \text{ m}^{-1/3}$
March 21, 1988	0.023	0.086	0.46	1.70
April 2, 1988	0.025	0.060	0.41	0.99

**Table 5. Measured angular deflections of P 0201 + 113 between March 21 and April 2, 1988.**

Observation time past March 21, 1988			DSS 13-43 measured deflection, nrad	DSS 15-43 measured deflection, nrad	Combined measured deflection, nrad	Expected deflection, nrad
hr	min	sec				
-00	19	40	2.63 ± 2.09	-0.42 ± 2.39	1.44 ± 1.69	3.21
00	22	14	2.29 ± 1.27	3.72 ± 0.90	3.52 ± 0.84	2.49
00	39	14	3.25 ± 1.18	2.85 ± 0.82	3.01 ± 0.78	2.21
00	56	17	1.00 ± 1.06	2.10 ± 0.76	1.86 ± 0.72	1.95
01	36	40	3.25 ± 1.28	0.99 ± 0.90	1.67 ± 0.84	1.38
01	54	05	3.10 ± 1.33	-0.05 ± 0.66	0.49 ± 0.63	1.18
02	11	06	0.75 ± 0.94	1.01 ± 0.65	1.06 ± 0.61	1.00
02	28	05	1.62 ± 0.99	-0.16 ± 0.65	0.35 ± 0.61	0.85
03	07	05	-0.79 ± 1.11	0.44 ± 0.66	0.28 ± 0.62	0.61
03	24	04	-1.51 ± 1.41	0.79 ± 0.77	0.47 ± 0.71	0.55

**Table 6. The  $\chi^2_\nu$  values for general relativity and no Jovian deflection hypotheses.**

Hypothesis	DSS 13-43 $\chi^2_\nu$	DSS 15-43 $\chi^2_\nu$	Combined $\chi^2_\nu$
General relativity	1.0	1.1	0.6
No Jovian deflection	2.8	3.7	4.1

**Table 7. Unmodeled error contributions to  $\delta \Delta s_p$ .**

Unmodeled effect	Error, nrad
Clock stochastics	0.05
Earth rotation stochastics	0.10
Solar deflection	0.10
Magnetosphere propagation	<0.01
Stationary source position/structure	0.24
Fluctuating source structure	0.10
Geophysical effects	0.10
Root-Sum-Square	0.32

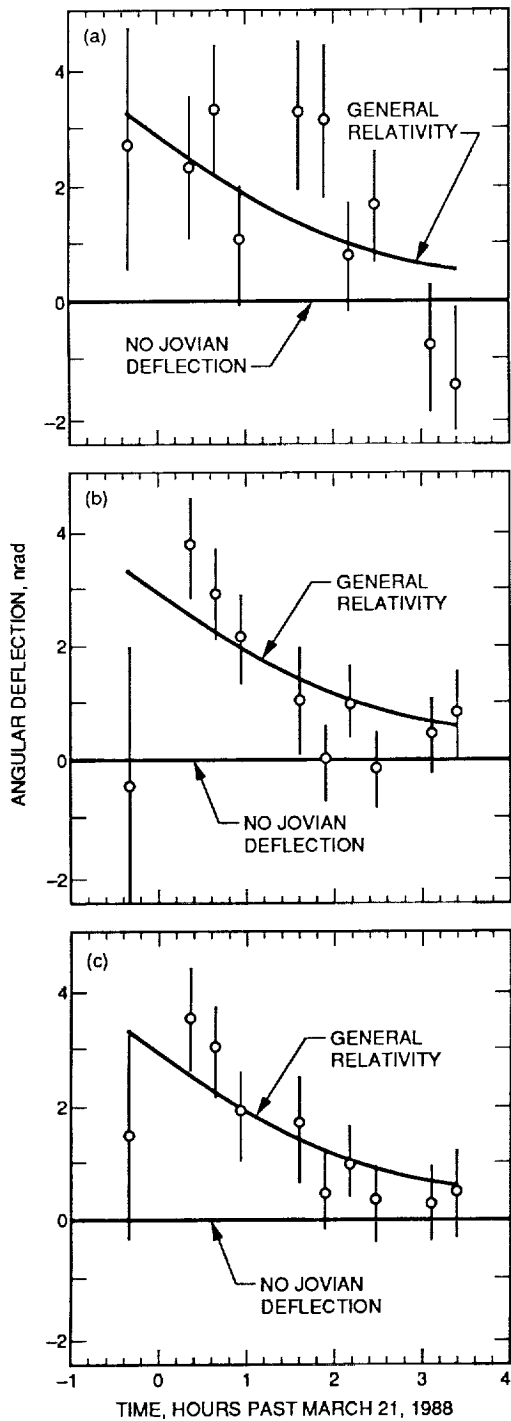


Fig. 1. The measured angular deflections, versus time, of the target radio source P 0201+113 between the March 21, 1988, and April 2, 1988, sessions for the DSS 13-43, DSS 15-43, and combined baselines, respectively. The curve in each figure is the baseline-projected deflection, versus time, caused by the changes in the target ray-paths' proximity to Jupiter between sessions, according to general relativity.

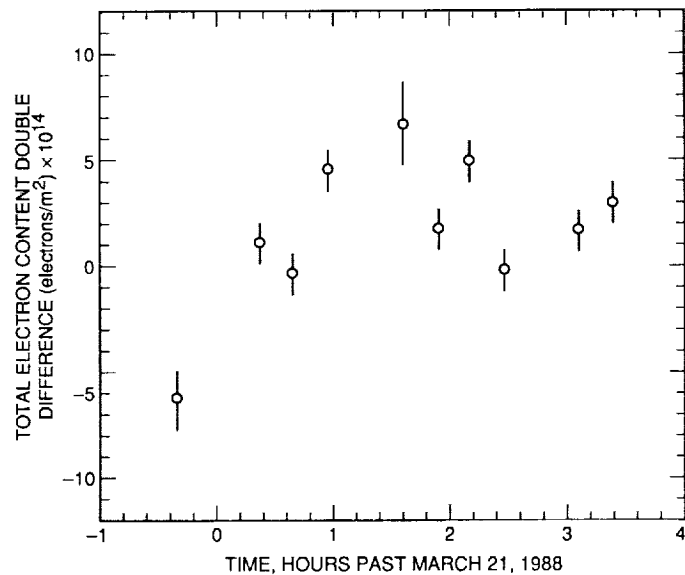


Fig. 2. The difference in measured electron columnar content between adjacent scans of the target, P 0201+113, and the closest reference source, P 0202+14, versus time, differenced between the March and April sessions. The columnar contents were inferred from the dual frequency VLBI data to investigate charged particle propagation effects through Jupiter's magnetosphere.